CHEMISTRY OF MATERIALS
Article

Chem. Mater. **2010,** *22,* 4669–4678 4669
DOI:10.1021/cm100874f

Atomic Layer Deposition of CdS Films

Jonathan R. Bakke,[†] Hee Joon Jung,[‡] Jukka T. Tanskanen,[†,§] Robert Sinclair,[‡] and Stacey F. Bent*[,†]

[†]*Department of Chemical Engineering, and* [‡]*Department of Materials Science and Engineering, Stanford University, Stanford, California 94305, and* [§]*Department of Chemistry, University of Eastern Finland, Yliopistokatu 7, 80130 Joensuu, Finland*

Received March 26, 2010. Revised Manuscript Received June 23, 2010

Pure, polycrystalline CdS deposited by atomic layer deposition (ALD) on Si(100) or glass using dimethyl cadmium and in situ generated H_2S is investigated in detail. This ALD system follows saturation behavior typical of ALD systems, and the growth rate monotonically decreases with temperature from 100 °C−300 °C; by 400 °C linear growth rate behavior is no longer seen. The crystal structure as determined by X-ray diffraction and transmission electron microscopy gradually transitions from zincblende to wurtzite with increasing temperature until the film is primarily wurtzite by 400 °C. Further, the average grain size increases with temperature. Transmission electron microscopy images and selected area diffraction patterns confirm the presence of zincblende and wurtzite crystals because of stacking faults and demonstrate that {111} crystal planes are more oriented parallel to the substrate at lower temperatures. Ultraviolet−visible spectroscopy shows that the bandgap is 2.3−2.42 eV in the 100 °C−400 °C range with a slight increase occurring with temperature. The roughness of the films is found to increase both with temperature and cycle number as observed with atomic force microscopy and scanning electron microscopy. Density functional theory calculations were used to understand observations concerning the growth rate and the bandgap of the films deposited at different temperatures.

Introduction

Atomic layer deposition (ALD) is a thin film growth technique with a myriad of applications because of its unique capabilities. Since the precursors are supplied sequentially into a reactor and the half-reactions are surface-reaction rate limited, ALD has the capability to produce uniform thin films over large areas at a maximum rate of one monolayer per cycle. Nevertheless, steric and/or electronic effects almost always lead to submonolayer growth (i.e., a rate lower than the interplanar distance per cycle). The ALD process is characterized by a growth rate that is linear as a function of the number of cycles even when an excess of precursor is dosed into the reactor.

CdS is a wide bandgap II−VI semiconductor with an energy gap of 2.42 eV,[1] and it is utilized for a number of applications. A primary use of CdS is as a buffer layer for thin film photovoltaic devices, and it is often deposited in zincblende form for these applications. In fact, the world record efficiencies for CdTe and $CuIn_xGa_{1-x}(S,Se)_2$ photovoltaics have been obtained with cells using CdS as the n-type buffer layer.[2] Applications of wurtzite CdS as a window for HgCdTe infrared detectors are especially interesting because of that crystal's long-term stability.[3] Recently, CdS quantum dots have gained attention for use in light emitting diodes and in photovoltaics as sensitizers.[4,5] CdS has been deposited by many methods[6] including chemical bath deposition,[7] atomic layer epitaxy (ALE),[8,9] metal organic chemical vapor deposition (MOCVD),[1,10,11] pulsed laser deposition,[12] and spray pyrolysis.[13] Various deposition methods using the dimethyl cadmium (DMCd) precursor have been used to deposit CdS and $Cd_xZn_{1-x}S$ films.[1,14]

The deposition of CdS via ALD has not yet been investigated under the normal operating conditions for most ALD systems; however, two earlier studies have described ALE of CdS in an ultrahigh vacuum (UHV) environment. Tadokoro et al. deposited CdS on GaAs-(100) under UHV with elemental Cd and S precursors by

*To whom correspondence should be addressed. E-mail: sbent@stanford.edu. Phone: (650) 723-0385. Fax: (650) 723-9780.

(1) Cockayne, B.; Wright, P. J. *J. Cryst. Growth* **1984**, *68*, 223–230.
(2) Repins, I.; Contreras, M. A.; Egaas, B.; DeHart, C.; Scharf, J.; Perkins, C. L.; To, B.; Noufi, R. *Prog. Photovoltaics* **2008**, *16*, 235–239.
(3) Boieriu, P.; Sporken, R.; Xin, Y.; Browning, N. D.; Sivananthan, S. *J. Electron. Mater.* **2000**, *29*, 718–722.
(4) Chang, C. H.; Lee, Y. L. *Appl. Phys. Lett.* **2007**, *91*, 3.
(5) Zhao, J. L.; Bardecker, J. A.; Munro, A. M.; Liu, M. S.; Niu, Y. H.; Ding, I. K.; Luo, J. D.; Chen, B. Q.; Jen, A. K. Y.; Ginger, D. S. *Nano Lett.* **2006**, *6*, 463–467.
(6) Mane, R. S.; Lokhande, C. D. *Mater. Chem. Phys.* **2000**, *65*, 1–31.
(7) Liu, Q.; Mao, G. B. *Surf. Rev. Lett.* **2009**, *16*, 469–474.
(8) Tadokoro, T.; Ohta, S.; Ishiguro, T.; Ichinose, Y.; Kobayashi, S.; Yamamoto, N. *J. Cryst. Growth* **1993**, *130*, 29–36.
(9) Luo, Y.; Han, M.; Slater, D. A.; Osgood, R. M. *J. Vac. Sci. Technol.* **2000**, *18*, 438–449.
(10) Obrien, P.; Walsh, J. R.; Watson, I. M.; Hart, L.; Silva, S. R. P. *J. Cryst. Growth* **1996**, *167*, 133–142.
(11) Yim, W. M.; Stofko, E. J. *J. Electrochem. Soc.* **1972**, *119*, 381.
(12) Ullrich, B.; Sakai, H.; Segawa, Y. *Thin Solid Films* **2001**, *385*, 220–224.
(13) Ma, Y. Y.; Bube, R. H. *J. Electrochem. Soc.* **1977**, *124*, 1430–1435.
(14) Bakke, J. R.; Bent, S. F. *ECS Trans.* **2009**, *25*, 9–14.

© 2010 American Chemical Society

ALE using a molecular beam epitaxy (MBE) setup at 340 °C. This system produced epitaxial c(200) CdS with stacking faults and dislocations.[8] Luo et al. deposited CdS by ALE at room temperature on ZnSe(100) using a UHV system as well.[9] The precursors dimethyl cadmium and H_2S were used to deposit up to 15 bilayers of stoichiometric CdS. Annealing at 250 °C produced zincblende CdS, which matched the substrate crystal structure. The reaction mechanism was also studied in detail, and the results showed that the DMCd precursor etched the surface to release DMZn. Another similar II−VI material, CdSe has been grown via ALE using cadmium and selenium elemental sources.[15]

In this study, we detail the deposition of CdS via ALD on hydroxyl terminated surfaces of Si(100) or glass using DMCd and an in situ H_2S source in an ALD flow reactor. In depth characterization of the growth rates of the films is performed, and DFT calculations are used to support observed growth rates. The material properties of the films including the crystal structure, bandgap, roughness, and surface morphology are carefully documented. In addition, we make direct comparisons between CdS ALD and the related ZnS ALD processes. ZnS is another II−VI semiconductor which has been studied more extensively when deposited by ALD. Analogous precursors dimethyl zinc (DMZn)[16] and diethyl zinc (DEZn)[17−19] have been used with the counter reactant H_2S to yield ZnS films, and density functional theory calculations have also been carried out to explore the growth mechanisms of ZnS.[20] Hence, it serves as an ideal basis for comparison.

Experimental and Computational Details

ALD growth of CdS was performed in a custom built warm wall reactor which has been described in a previous publication.[17] The precursors for this reaction were dimethyl cadmium (DMCd) (Strem)[14] and in situ generated H_2S which is produced by heating thioacetamide to 150 °C under an inert atmosphere; this method has been previously described in detail.[17] DMCd is a liquid at room temperature with a melting point of −4.5 °C and a boiling point of 105.5 °C at atmospheric pressure. DMCd is a highly reactive chemical and should only be handled in a glove box free of water and oxygen. The H_2S is mostly pure with small amounts of acetonitrile. Nitrogen was used as the carrier and purge gas at a constant flow rate of 60 sccm. The substrate temperature was varied for the deposition of CdS with the temperature affecting parameters such as growth rate, crystal structure, root-mean-square (rms) roughness, and bandgap. For all studies except pulse and purge length dependencies, the optimized cycle of ALD consisted of 0.4 s DMCd, 10 s purge, 0.4 s H_2S, and a 10 s purge. All precursors were maintained at room temperature (∼22 °C). Needle valves controlled the rate of dosing of each precursor.

The substrate for ellipsometry, scanning electron microscopy (SEM), atomic force microscopy (AFM), X-ray photoelectron spectroscopy (XPS), and transmission electron microscopy (TEM) measurements was a Czochralski grown n-type Si(100) wafer with a resistivity of 1−5 Ω-cm and a native silicon oxide layer which is approximately 2 nm thick. Films were also deposited on glass for comparison of crystal orientation and bandgap using X-ray diffraction (XRD) and ultraviolet−visible spectroscopy (UV−vis), respectively. The substrates were cleaned via 5 min sonication steps each in acetone and ethanol with deionized water rinses between each solvent bath. Residual organics were then removed with a piranha clean (70% sulfuric acid and 30% hydrogen peroxide) for 15 min followed by a deionized water rinse and drying with pressurized air. Fresh piranha is hot and corrosive, and extreme caution must be used when handling this solution.

After ALD, resulting film thicknesses were measured by a Gaertner L116C single-wavelength ellipsometer using 632.8 nm light at a 70° angle of incidence and with the polarizer set to 45°. At least two 1 cm ×1 cm samples from each run were used, and measurements were performed on three spots for each sample to account for any non-uniformity. Elemental composition of the films was determined by XPS with a Surface Science Instruments S-Probe monochromatized spectrometer using Al Kα 1486 eV radiation at a pressure of 6.7×10^{-11} kPa (5×10^{-10} Torr). The Argon sputter was performed at a pressure of 1.3×10^{-8} kPa (1×10^{-7} Torr) using 5 keV Ar^+ at 2 mm × 2 mm raster at 45° incidence to the sample. Survey scans were performed with a step size of 1 eV. Surface morphology and roughness were characterized with a Veeco Multimode AFM in tapping mode with MikroMasch NSC16 tips. Crystal structure was determined with a PANalytical X'Pert PRO XRD system in parallel beam mode using Cu Kα radiation. Surfaces were imaged by SEM using an FEI XL30 Sirion SEM at a 5 kV operating voltage. Bandgaps were determined by UV−vis with Varian's Cary 6000i UV−vis−NIR spectrophotometer. TEM samples with a thickness of ∼80 nm were prepared using a focused ion beam (FIB, FEI Strata 235DB dual-beam FIB/SEM) lift-out Omniprobe technique with a Ga^+ ion beam at 30 keV. Cross-sectional bright-field and high resolution transmission electron microscopy images and selected area diffraction (SAD) patterns were taken by an FEI Tecnai G2 F20 X-TWIN operated at an accelerating voltage of 200 kV. Fast Fourier Transformation (FFT) images were obtained by DigitalMicrograph from the high resolution TEM (HRTEM)

Periodic hybrid density functional theory (DFT) calculations were performed to investigate the electronic characteristics of the deposited films and the temperature dependence of the growth rate. The calculations were carried out by CRYSTAL2006[21] quantum chemistry software using the PBE0 density functional,[22] which is one of the better performing hybrid functionals for solid state and for late-transition-metal reactions.[23,24] Default optimization convergence thresholds and an extra large integration grid were utilized in the calculations. Karlsruhe split-valence basis set with polarization functions (def2-SVP)[25] was used for C and H, while a standard 6-31G* basis was adopted for S. For Cd a triple valence quality

(15) Mikhaevich, D. P.; Ezhovskii, Y. K. *Russ. J. Appl. Chem.* **2003**, *76*, 1197–1200.
(16) Hunter, A.; Kitai, A. H. *J. Cryst. Growth* **1988**, *91*, 111–118.
(17) Bakke, J. R.; King, J. S.; Jung, H. J.; Sinclair, R.; Bent, S. F. *Thin Solid Films* **2010**, *518*, 5400–5408.
(18) Kim, Y. S.; Yun, S. J. *Appl. Surf. Sci.* **2004**, *229*, 105–111.
(19) Stuyven, G.; De Visschere, P.; Hikavyy, A.; Neyts, K. *J. Cryst. Growth* **2002**, *234*, 690–698.
(20) Tanskanen, J. T.; Bakke, J. R.; Bent, S. F.; Pakkanen, T. A. *Langmuir* **2010**, *26*, 11899−11906.
(21) Dovesi, R. S.; Saunders, V. R.; Roetti, C.; Orlando, R.; Zicovich-Wilson, C. M.; Pascale, F.; Civalleri, B.; Doll, K.; Harrison, N. M.; Bush, I. J.; D'Arco, Ph.; Llunell, M. *CRYSTAL2006 User's Manual*; University of Torino: Torino, Italy, 2006.
(22) Adamo, C.; Barone, V. *J. Chem. Phys.* **1999**, *110*, 6158–6170.
(23) Paier, J.; Marsman, M.; Kresse, G. *J. Chem. Phys.* **2007**, *127*, 24103.
(24) Quintal, M. M.; Karton, A.; Iron, M. A.; Boese, A. D.; Martin, J. M. L. *J. Phys. Chem. A* **2006**, *110*, 709–716.
(25) Weigend, F.; Ahlrichs, R. *Phys. Chem. Chem. Phys.* **2005**, *7*, 3297–3305.

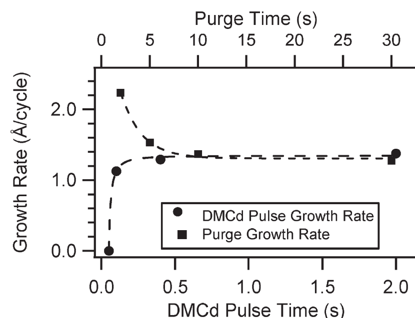

Figure 1. CdS growth rate on Si(100) as a function of DMCd pulse time and N_2 purge time. 100 cycle films were deposited at 150 °C. Purge time was 10 s and H_2S pulse time was 0.4 s for the DMCd pulse study, and pulse times for H_2S and DMCd were 0.4 s for the purge time study.

9−7−6-311-d631G basis[26,27] with the outermost exponent variationally optimized for bulk CdS (0.1739 − > 0.1797) was used. A modified basis set was necessary for the periodic calculations, and the basis reproduced the characteristics of bulk CdS well. As an example, the optimized lattice parameter of zincblende CdS was within 2% of the experimental value. The active growth surface was modeled by a four atomic layer thick hydrogenated S-terminated (111) slab of zincblende CdS, and the outermost atomic layer of the slab was allowed to relax in the optimizations. Frequency calculations were performed to investigate the effect of thermodynamics on the film growth characteristics. The electronic characteristics of the deposited films were analyzed on the basis of PBE0-calculated density of states-plots (DOS) and by using 2 × 2 × 2 and 3 × 3 × 3 CdS supercells with a stoichiometry of Cd_8S_8 and $Cd_{27}S_{27}$, respectively. The expansion of the DOS plots was performed using 18 Legendre polynomials.

Results and Discussion

1. ALD Growth Characterization. CdS growth rates as a function of precursor pulse time and nitrogen purge time were studied, keeping all other process parameters constant. The resulting growth rate curves are shown in Figure 1 as a function of DMCd pulse time and N_2 purge time, respectively. The data in Figure 1 show that saturation behavior, which is a characteristic of ALD, with respect to DMCd is reached by 0.4 s, and the growth is self-limiting. Also shown, after 10 s of purging with N_2, excess reactants have been removed. The growth rate dependence on H_2S pulse time was not measured since the gas was delivered in excess to account for a decrease in the pressure of H_2S gas during deposition. Unless otherwise stated, experiments in this paper were performed at the optimum conditions for 150 °C, which is a pulse sequence of 0.4 s DMCd, 10 s N_2 purge, 0.4 s H_2S, and 10 s N_2 purge with a total nitrogen flow rate of 60 sccm. A purge time of around 7 s is sufficient in this reactor for ALD growth; however, a 10 s purge time was used to ensure that no CVD component is incorporated during the detailed study of ALD growth rate and properties.

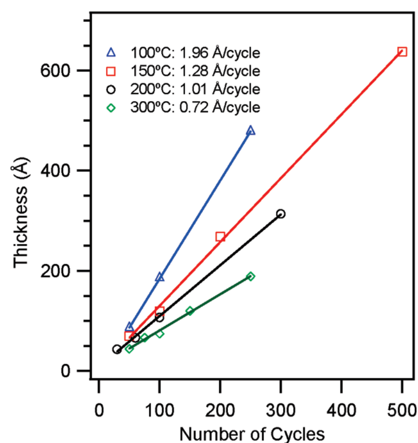

Figure 2. Film thickness as a function of temperature for CdS ALD.

Using the optimized operating parameters at 150 °C described above, the behavior of the CdS deposition process was tested over a temperature range of 100 °C−400 °C. Figure 2 demonstrates that the growth is linear for the 100 °C−300 °C range. The growth rates obtained by linear regression decrease with temperature, and DFT calculations provide an explanation for this effect (vide infra). The growth rate monotonically decreases from approximately 1.96 Å/cycle at 100 °C to 0.72 Å/cycle at 300 °C. These growth rates are equivalent to 0.58 monolayers/cycle and 0.21 monolayers/cycle, respectively, when referenced to the c(111) interplanar distance of 3.36 Å. At 300 °C a significant portion of the film has the h(103) phase, and the growth rate is 0.38 monolayers/cycle using its interplanar distance of 1.9 Å; consequently, the actual growth rate at 300 °C is in the range of 0.21−0.38 monolayers/cycle. No incubation period is evident from the growth rate studies indicating that nucleation occurs fairly readily on the SiO_2/Si(100) substrate; nevertheless, further experiments specifically focusing on nucleation are of interest for future studies.

The boiling point of DMCd is 105.5 °C, and an increased residence time in the reactor at lower temperatures may account for the significantly increased growth rate at 100 °C because the remaining reactant could react with H_2S during the following pulse, leading to a small CVD component. However, as shown by Groner et al. for deposition of Al_2O_3 using trimethylaluminum at low temperatures, the growth rate can be held constant by increasing the purge time at lower temperatures.[28] At 400 °C, the growth rate does not display the linear behavior expected from ALD: the growth rate increases with cycle number and is not uniform across a 2 in. sample range. This observation is likely due to instability or decomposition of the ligands. Thus, true ALD does not occur at 400 °C, but pure CdS is still deposited without contamination from ligands. The cross-section TEM images in Figure 3a confirm the growth rate for the 150 °C film. The thickest portion of the 400 °C film was analyzed by TEM, and it verifies that the film is very rough.

(26) *CRYSTAL basis set library at* http://www.crystal.unito.it/Basis_Sets/Ptable.html.
(27) Dou, Y.; Egdell, R. G.; Law, D. S. L.; Harrison, N. M.; Searle, B. G. An experimental and theoretical investigation of the electronic structure of CdO. *J. Phys.: Condens. Matter* **1998**, *10*(38), 8447–8458.
(28) Groner, M. D.; Fabreguette, F. H.; Elam, J. W.; George, S. M. *Chem. Mater.* **2004**, *16*, 639–645.

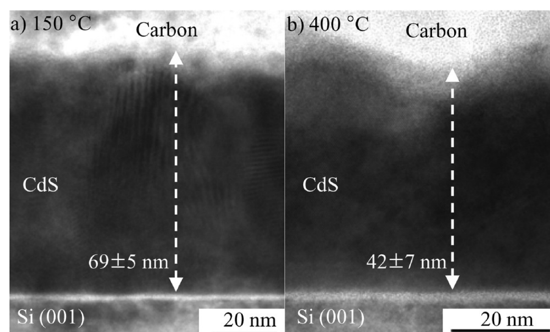

Figure 3. TEM images of 500 cycles of CdS at (a) 150 °C and (b) 400 °C.

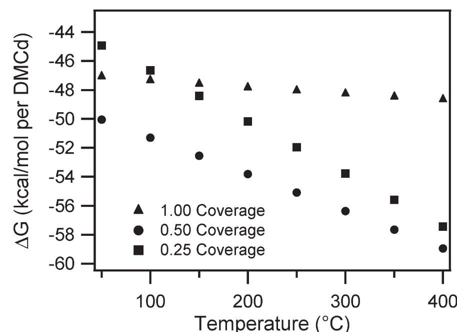

Figure 4. PBE0-calculated dissociative DMCd chemisorption energies per precursor (ΔG, 1 atm) on hydrogenated S-terminated (111) surface of zincblende CdS for a precursor fractional surface coverage of 0.25, 0.50, and 1.00 as a function of temperature.

The growth rate curves obtained for CdS display many similarities to the diethylzinc and H_2S ALD process.[17] The ZnS system displays a growth rate that monotonically decreases with temperature from a rate of 0.44 monolayers/cycle at 100 °C to 0.24 monolayers/cycle at 300 °C (compared to 0.58 monolayers/cycle and 0.21 monolayers/cycle for CdS). Moreover, density functional theory calculations by Tanskanen et al.[20] suggest that a higher growth rate occurs with DMZn compared to DEZn. Consequently, the increased growth rate in terms of Å/cycle is not unexpected compared to the DEZn system because of the increased lattice constant and the difference in ligands. Also, neither system shows a "traditional" ALD window in which the growth rate is flat.[17,19]

To understand the origin of the decreasing growth rate as a function of increasing temperature, the film growth characteristics were investigated by periodic PBE0 calculations. We focused on studying the reaction energies for the dissociative chemisorption of DMCd according to the reaction mechanism $SH^*(s) + Cd(CH_3)_2(g) \rightarrow S{-}Cd{-}CH_3^*(s) + CH_4(g)$, which has been suggested to be the major pathway of DMCd dissociation with a hydrogenated sulfur surface where "*" refers to the surface species.[29] The SH*(s) growth surface was represented by a hydrogenated (111) slab of cubic CdS, and precursor surface coverages of 0.25, 0.50, and 1.00 monolayers were considered. The calculated Gibbs-corrected reaction energies at temperatures between 50 and 400 °C are illustrated in Figure 4. The energies are given per mole of precursor to allow direct comparison of different fractional coverages. At low temperatures, the DMCd dissociation energies for the different coverages are within 5 kcal/mol of each other. On the other hand, low-coverage systems become clearly favored over a monolayer coverage as a function of increasing temperature so that by 400 °C the surface coverages of 0.25 and 0.50 are favored over the full coverage system by approximately 10 kcal/mol per chemisorbed DMCd. As a consequence, the slow growth rates at high temperatures are attributed to partial surface coverage by the metal precursor because of steric hindrance at highly covered surfaces. The calculated energetic trends originate primarily from (1) entropy and (2) steric effects: (1) Namely, atomic motion, which increases as a function of temperature, is more limited for the tightly packed monolayer with respect to the lower fractional coverages, and thus entropy increases at an increasing rate for the lower coverages with temperature. (2) In addition, the effective size of the chemisorbed species increases with temperature because of the increased atomic motion, which leads to more significant ligand repulsion at higher coverages and to the observed preference for the less densely packed surfaces at higher temperatures.

2. Film Characterization. XPS was used to analyze the composition of the ALD films and shows that the films are stoichiometric to within the error of the XPS method; the chemical composition as calculated from XPS data is bounded by a few atomic percent because of the many sources of error inherent in quantitative analysis by XPS;[30−32] moreover, the cross-section (sensitivity) for Cd in XPS is much larger than for S.[33] Thus, films deposited above 150 °C are likely stoichiometric as the bandgap and crystal lattice parameters match that of pure CdS (vide infra). Films deposited at 100 °C display behaviors which may be due to sulfur vacancies or hydrogen impurities (vide infra) and are not unexpected from literature.[28,34] Figure 5 shows an XPS spectrum of a film deposited at 200 °C: only Cd and S are visible in the film. Similar to the ZnS deposition in a previous study,[17] no noticeable carbon or nitrogen from the acetonitrile byproduct of the in situ H_2S generation is incorporated into the film. No contaminants were seen in any analyzed samples in the temperature range of 100 °C−400 °C, and the composition did not change with temperature. Finally, the composition was analyzed at various sputter times, and the composition was constant, confirming that the sputtering did not have a noticeable effect on the measured composition.

CdS is well-known to exist in either the zincblende (cubic) or the wurtzite (hexagonal) crystal structures, and the phase strongly depends upon factors

(29) Han, M.; Luo, Y.; Moryl, J. E.; Osgood, R. M. *Surf. Sci.* **1999**, *425*, 259–275.
(30) *Analytical Instrumentation Handbook*; Marcel Denker: Las Vegas, NM, 1990.
(31) Ohring, M., *The Materials Science of Thin Films*; Academic Press Limited: New York, 1992.
(32) Wagner, C. D. *Anal. Chem.* **1977**, *49*, 1282–1290.
(33) Wagner, C. D.; Davis, L. E.; Zeller, M. V.; Taylor, J. A.; Raymond, R. H.; Gale, L. H. *Surf. Interface Anal.* **1981**, *3*, 211–225.
(34) Weber, M.; Krauser, J.; Weidinger, A.; Bruns, J.; Fischer, C. H.; Bohne, W.; Rohrich, J.; Scheer, R. *J. Electrochem. Soc.* **1999**, *146*, 2131–2138.

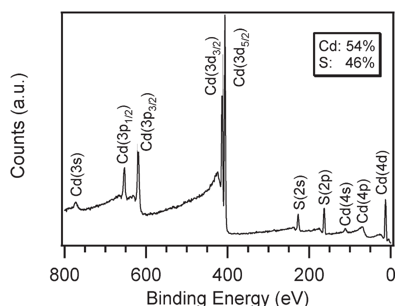

Figure 5. XPS survey spectrum after 10 s Ar^+ ion sputter of CdS film deposited at 200 °C.

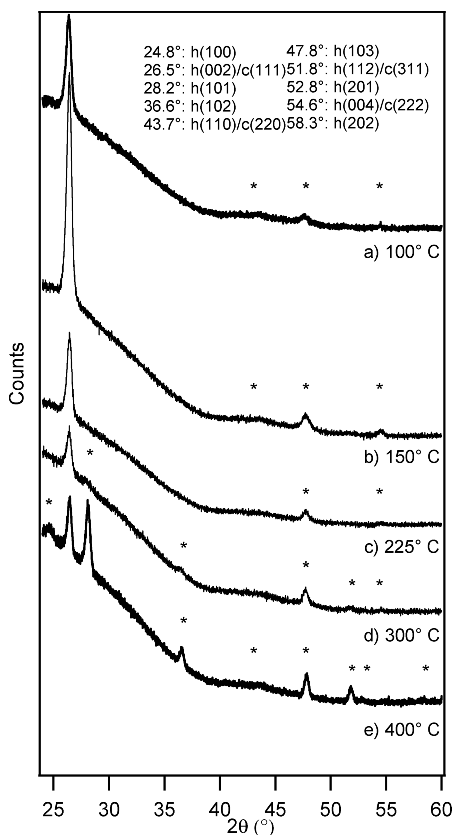

Figure 6. Temperature dependent XRD patterns of CdS on glass. The patterns correspond to (a) 100 °C (49 nm) (b) 150 °C (64 nm), (c) 225 °C (29 nm), (d) 300 °C (28 nm), and (e) 400 °C (37 nm). Asterisks designate a peak. The peak at 26.5° is not labeled with a star.

such as deposition method, temperature, time, and precursors.[3,7,9,10,35] The crystal structure in this work was determined by XRD for CdS films grown at temperatures ranging from 100−400 °C on glass. The data is summarized in Figure 6, and peaks are labeled with a "*". All CdS films share two peaks, one at 26.5° corresponding to the h(002)/c(111) peak and one at 47.8° corresponding to h(103). The large background slope at low intensities is due to the amorphous glass substrate. Table 1 provides a summary of the relative intensities of each peak and compares this ALD system to that of the similar ZnS system.

At lower temperatures, the films are primarily zincblende, and the wurtzite content increases with temperature. The phase change is gradual from 100 to 300 °C with the films over this temperature range primarily containing zincblende CdS. A large shift from zincblende to mostly wurtzite occurs by 400 °C as signified by the strong appearance of the h(101) peak at 28.2°and an increase of intensity in the h(103) peak. The wurtzite XRD pattern is similar to patterns obtained from wurtzite films or nanoparticles deposited by other methods.[36] The difference in peak intensities of the main peak at 26.5° at different deposition temperatures is due to several reasons. First, there are slight differences in the thickness (see Figure 6 caption) that largely account for the change in intensities. Next, as both phases appear in the thin film, the average intensity of this peak decreases. Finally, as discussed in detail for a ZnS system, the tendency for{111} planes of zincblende to preferably align parallel to the sample surface decreases with increasing temperature.[17] The crystal structure presented herein is strongly dependent on the deposition temperature. The 100 and 400 °C samples were annealed at 500 °C in a pure H_2S atmosphere and no change occurred in the XRD patterns (data not shown).

Using the Scherrer equation and the full width half max (fwhm) of the peak intensity for the main peak at 26.5°, the average grain size for the main crystal grains can be estimated; however, it should be noted that the Scherrer equation provides a minimum average crystal size because of line broadening that may occur from the equipment. The results of this analysis, shown in Figure 7, indicate that the grain size linearly increases with temperature. We can also analyze the average grain size of the wurtzite crystal structure obtained from the 47.8° peak which is present in all the films (Figure 9). The grain sizes at lower temperatures are small at ∼12 nm; however, the size quickly increases at 225 °C and increases with temperature thereafter. This examination shows that at low temperatures the wurtzite grains are small, and this phenomenon is attributed to their formation from stacking faults in the cubic structure (vide infra). At higher temperatures, the main growth mechanism forms wurtzite so the grains are larger. The film thickness (given in the Figure 6 caption) does not appear to significantly affect the grain size. To confirm the above trends in crystal size, the crystal sizes were analyzed from cross-section TEM images (vide infra), and the crystals were determined to be 11 ± 3 nm at 150 °C and 29 ± 16 nm at 400 °C. As mentioned before, XRD patterns of the 150 and 400 °C films after a 10 h anneal in H_2S at 500 °C were analyzed, and the phases present did not change; however, the average grain size as determined by the fwhm for the 150 °C film increased to be equivalent to that obtained for the as deposited 400 °C film. The grain sizes did not change for the 400 °C sample after annealing.

A comparison to the ZnS ALD system as shown in Table 1 demonstrates that for CdS films, wurtzite

(35) Froment, M.; Bernard, M. C.; Cortes, R.; Mokili, B.; Lincot, D. *J. Electrochem. Soc.* **1995**, *142*, 2642–2649.

(36) Singh, V.; Chauhan, P. *Chalcogenide Lett.* **2009**, *6*, 421–426.

Table 1. Summary of CdS XRD Intensities Relative to the h(002)/c(111) Peak and a Comparison to an Analogous ZnS ALD Process[a]

		400 °C		300 °C		225 °C		150 °C		100 °C	
cubic	hexagonal	CdS	ZnS	CdS	ZnS	CdS	ZnS	CdS	ZnS	CdS	ZnS
	100	0.14									
111	002	1.00	1.00	1.00	1.00	1.00	1.00	1.00	1.00	1.00	1.00
	101	1.20		0.14							
200			0.02								
	102	0.30		0.13							
220	110	0.06	0.05		0.01		0.003	0.02		0.03	
	103	0.41	0.06	0.44	0.07	0.13	0.003	0.06	0.002	0.08	
311	112	0.23	0.10	0.14	0.02		0.003				
	201	0.07									
222	004			0.08	0.01	0.03	0.01	0.03	0.01	0.05	
	202	0.06									
%h(002)/c(111)		29%	79%	52%	90%	86%	98%	90%	99%	86%	100%

[a] The %h(002)/c(111) row is the percentage of total intensity belonging to that peak.

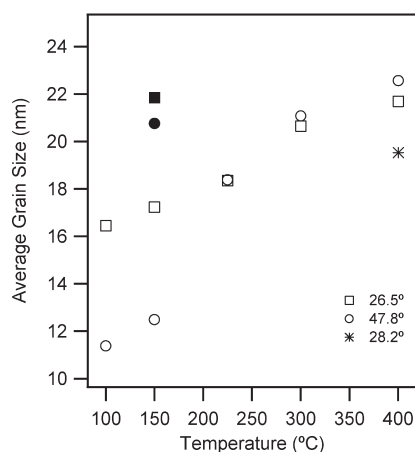

Figure 7. Grain sizes of the main grains attributed to the principal cubic and wurtzite peaks. The solid markers are measured after a 500 °C anneal in H_2S for 10 h.

characteristics are displayed at lower temperatures and also increase at a much faster rate with increasing temperature. For example the h(002)/c(111) peak accounts for 100% and 79% of the intensity for ZnS films at 100 and 400 °C, respectively. However, in CdS films the values are 87% and 29%. If one accounts for the peaks that are solely attributable to wurtzite phases, the CdS and ZnS films at 400 °C are at least 63% and 5% wurtzite, respectively. In fact, the h(101) peak dominates for CdS at 400 °C. The increased stability of the wurtzite phase in CdS compared to ZnS has been shown in a previous study where the phase of the $Cd_xZn_{1-x}S$ at a constant temperature is strongly affected by the composition.[37]

The crystal grain growth is confirmed to be distinct at different temperatures by studying the TEM images in Figure 3 and the SAD patterns in Figure 8, and they are supported by the XRD patterns in Figure 6. Large columnar zincblende grains for the 150 °C film extending from the surface are visible in the TEM image in Figure 3a, and the SAD pattern over Si and CdS using a 150 nm diameter aperture shown in Figure 8a corroborates that the zincblende (111) planes are highly oriented parallel to the surface since the CdS zincblende

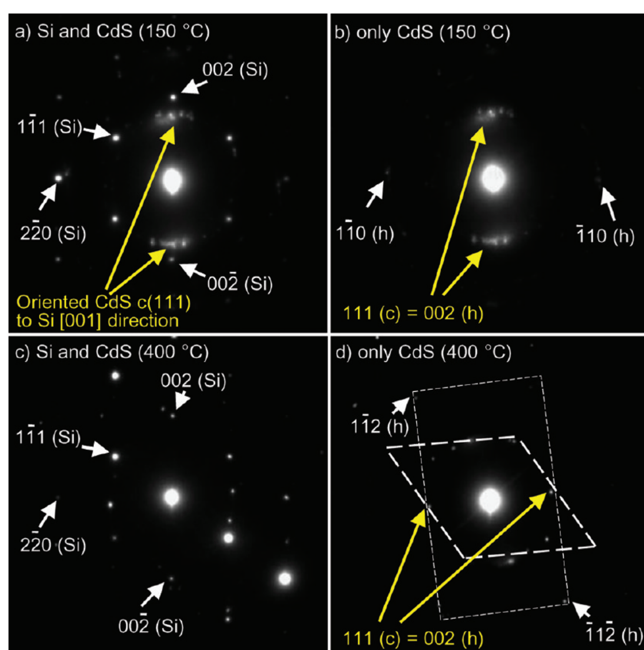

Figure 8. Selected area diffraction (SAD) patterns of 500 cycle films of CdS with 150 nm diameter aperture at 150 °C (a and b) and at 400 °C (c and d): a and c SAD patterns are of Si and CdS, b and d SAD patterns are of CdS only. The SAD pattern in b for 150 °C shows mainly zincblende spots and the CdS (111) planes are strongly oriented parallel to the film surface (underlying substrate is Si (001). The SAD in d for 400 °C shows that zincblende (111) planes and wurtzite (002) planes have same directional stacking which is evidence for stacking fault formation in the wurtzite phase. The preferential orientation of crystals is lost at 400 °C compared to 150 °C.

(111) spots are aligned to the Si (002) spots (present because of dynamical diffraction) with bright intensity. This alignment may also be inferred from Figure 6b because of the presence of only one high intensity X-ray peak in the pattern corresponding to c(111). Very weak intensity wurtzite 1$\bar{1}$0 (h) type spots in the SAD pattern in Figure 8b confirm the XRD analysis that there is a small portion of wurtzite phase present in films deposited at 150 °C. The SAD pattern contains spots which are primarily a contribution from the c(111) crystals strongly oriented to the Si (002) direction. An HRTEM image and its FFT image (not shown) further confirm that both wurtzite and zincblende crystals are present in the 150 °C film. In Figure 8 various diffraction spots of zincblende

(37) Chen, W. W.; Zhang, J. M.; Ardell, A. J.; Dunn, B. *Mater. Res. Bull.* **1988**, *23*, 1667–1673.

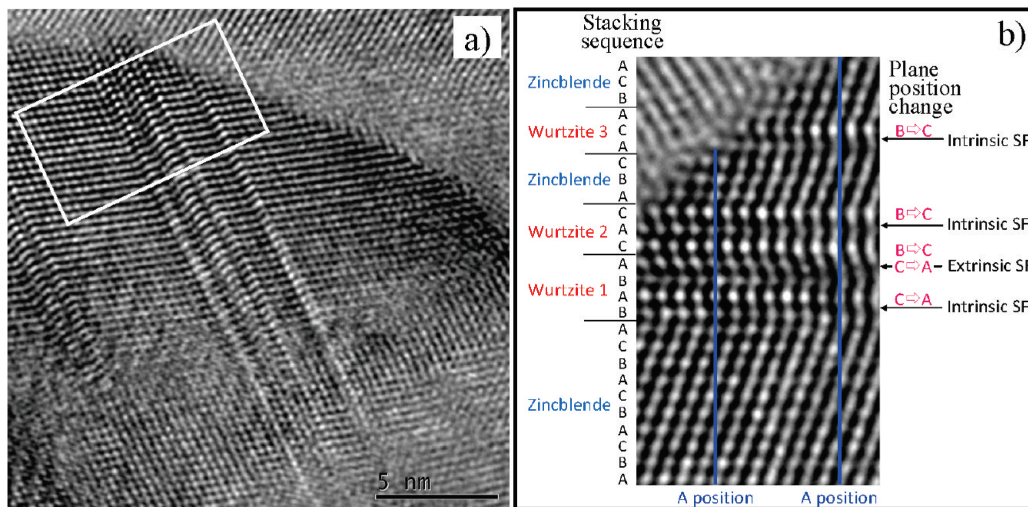

Figure 9. High resolution TEM image of 150 °C CdS film: (a) overview of a grain containing stacking faults and (b) magnified view of the region in the white box in (a). Intrinsic and extrinsic stacking faults (SFs) form by a/6 $\langle 2\bar{1}\bar{1}\rangle$ type displacement of plane position on zincblende (111) planes to form local wurtzite grains. Closely spaced SFs may construct a larger wurtzite structure.

and wurtzite were assigned on the basis of the previously reported lattice parameters[36,38] by the relationship of $Rd = L\lambda =$ fixed constant, which is the camera length equation of a TEM diffraction pattern, where R is the distance from the center spot to a specific spot corresponding to a specific plane, d is the interplanar spacing between the specific planes, L is the camera length, and λ is 2.51 pm, which is the wavelength of the electron beam with a 200 kV acceleration. The Si spots in the SAD patterns of Figure 8a and Figure 8c were used as a reference because Si has a well-known lattice parameter (a_{Si} = 5.4308), and direct comparison of the spots between Si and CdS gives better verification of CdS spots.

Comparatively, the 400 °C film does not show a strong alignment of the h(002)/c(111) planes and is primarily wurtzite in character. The XRD patterns and Table 1 show that many crystal phases are visible because of the random orientation. The SAD patterns such as those in Figure 8c,d show that the crystals are randomly oriented compared to the silicon substrate. Thus, the reduction in peak intensities of the main peak as seen in XRD is due to both the increasing wurtzite content and the decreasing texture. The clear wurtzite diffraction array with higher index planes is seen in the SAD pattern of the CdS region in Figure 8d. c(111) and h(002) have the same diffraction spot position because the ABC stacking direction of the c(111) planes is the same as the AB stacking direction of h(002) planes. This coincidence of c(111) and h(002) suggests the presence of stacking faults which local form hexagonal stacking in the cubic structure. Random orientation of the spots without coincidence would signify that wurtzite forms freely without orientation relative to zincblende; thus, the coincidence of those spots is consistent with wurtzite AB stacking resulting from stacking faults in the zincblende ABC stacking. Further, the clearer and stronger intensity of the wurtzite diffraction spots in Figure 8d as opposed to Figure 8b presumably indicates a higher portion of wurtzite in that local area. An HRTEM image of the 400 °C film and its FFT image (not shown) elucidate that both zincblende and wurtzite CdS are present. The SAD pattern matches the FFT image in that the c(111) plane is coincident with the h(002) plane.

A high resolution TEM image of 150 °C CdS film (Figure 9a) confirms that wurtzite grains are present in zincblende grains because of stacking faults. A magnified view of the HRTEM image in Figure 9b shows mixed local zincblende and wurtzite form from a combination of intrinsic and extrinsic stacking faults, and the stacking sequence is clearly defined and labeled. c(111) and h(002) planes are stacked parallel and a/6 $\langle 2\bar{1}\bar{1}\rangle$ type displacement of zincblende (111) planes yields intrinsic and extrinsic stacking faults which provide transformation from zincblende (thermodynamically stable phase at 150 °C) to wurtzite (metastable phase at 150 °C). This indicates that wurtzite AB stacking forms because of stacking faults from zincblende ABC stacking. Finally, closely spaced stacking faults can construct a larger local wurtzite structure as seen in Figure 9b.

Optical characterization of the CdS films on glass was performed with UV−vis to determine the bandgap. CdS is a direct bandgap semiconductor, and literature values of the bandgap range from 2.25 eV−2.45 eV depending on deposition method, crystal structure, grain size, and quantum effects;[1,7,12,36,39] however, the accepted bandgap for pure CdS is 2.42 eV.[1] CdS quantum dots display much larger bandgaps; however, they approach bulk values at >10 nm, which means significant quantum confinement effects are not expected for these films based on the Scherrer equation calculations.[40,41] In this work,

(38) Benkabou, F.; Aourag, H.; Certier, M. *Mater. Chem. Phys.* **2000**, *66*, 10–16.
(39) Zelayaangel, O.; Hernandez, L.; Demelo, O.; Alvaradogil, J. J.; Lozadamorales, R.; Falcony, C.; Vargas, H.; Ramirezbon, R. *Vacuum* **1995**, *46*, 1083–1085.
(40) Wang, Y.; Herron, N. *Phys. Rev. B* **1990**, *42*, 7253.
(41) Weller, H. *Angew. Chem., Int. Ed. Engl.* **1993**, *32*, 41–53.

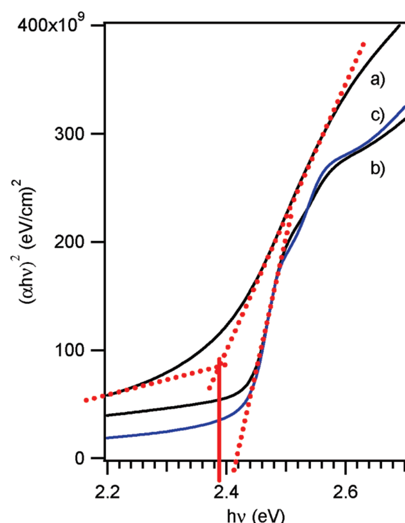

Figure 10. Tauc plots (a) of as deposited CdS at 150 °C and (b) of the same film after a 500 °C anneal in an H_2S atmosphere and (c) of as deposited CdS at 400 °C.

Tauc plots of $(\alpha h\nu)^2$ versus $h\nu$ are used to estimate the bandgap for several thicknesses and ALD temperatures. The Tauc plots for 500 cycle films deposited at 150 and 400 °C are shown in Figure 10. For films deposited at 100 and 150 °C, the bandgap is ∼2.3 eV, and for films deposited in the range 225 °C−400 °C, the bandgap exactly matches the literature value of 2.42 eV. The thickness did not appear to have an effect on the bandgap.

An interesting observation is that an inflection point appears in the Tauc plot over the 2.5−2.6 eV range for films deposited between 225−400 °C because of a new absorption edge that occurs at ∼2.5 eV. The high absorption energy is probably due to the increased wurtzite content in the films deposited at higher temperatures, which would be similar to observations for the ZnS system using DEZn/H_2S.[17] The 150 and 400 °C films were also annealed at 500 °C in an H_2S atmosphere for 10 h to study the difference compared to the as deposited films. After the anneal, UV−vis spectroscopy and XRD were performed again on the samples. According to XRD, no significant alteration in crystal structure occurred for either film, but the grain sizes appeared to increase for the 150 °C film (vide supra). On the other hand, Zelaya-Angel et al. noted that zincblende CdS deposited by CBD transitioned to wurtzite upon a 500 °C anneal;[39] that effect was not observed here. The bandgap of the 400 °C film remained unchanged; however, Figure 10b illustrates that the optical characteristics of the 150 °C film significantly changed in three ways. First, the bandgap blue-shifts to 2.42 eV matching that of the films deposited at higher temperatures. Second, the Tauc plot also displays the inflection points at ∼2.5 eV because of the presence of a new absorption edge. Finally, the slope at energies below the CdS absorption is flat like that for the as deposited 400 °C film and the annealed films. The as deposited 150 °C film, however, shows a gradual change in slope at energies below the CdS bandgap. If the Tauc plot for Figure 10a is baselined to account for this, the "bulk" bandgap shifts closer to the bandgap for the annealed and 400 °C films.[42] This gradual change in the bandgap may be related to the less crystalline nature of the 150 °C film as discussed above with the XRD patterns and Scherrer equation calculations, or it may be related to the presence of some sulfur vacancies in the film (vide infra). These vacancies may also serve to "wash out" the absorption due to the wurtzite crystals since they are present in Figure 10b after the H_2S anneal.

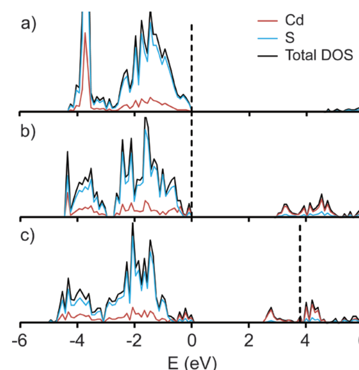

Figure 11. PBE0-calculated projected and total DOS plots using a 2 × 2 × 2 supercell for cubic CdS. (a) Defect-free CdS, (b) S vacancy density of 1.7 nm^{-3}, (c) S substitution density of 1.7 nm^{-3}. Fermi levels are indicated with dashed lines.

DOS plots for zincblende CdS were calculated at the PBE0 level of theory to determine if the described bandgap behavior of the films deposited at 150 °C could be explained by a model in which defects affect the bandgap at 150 °C but are removed upon annealing. As previously noted by XPS (see Figure 5), the films may be slightly rich in cadmium. Two possible routes for excess cadmium were modeled: one due purely to sulfur vacancies and another due to cadmium substitutions. The calculated defect densities were 1.7 defects·nm^{-3} and 0.5 defects·nm^{-3}. The calculated total DOS plots with contributions from S and Cd are shown for the 1.7 nm^{-3} defect densities in Figure 11. The S vacancies have an effect on the electronic structure of CdS by introducing mainly Cd states to the valence region and decreasing the optical gap with respect to zincblende CdS. The bandgap is decreased by 0.4 eV when the S vacancy defect density is 0.5 nm^{-3} compared to a pure CdS film. Substitution of S by Cd has a strong impact on the electronic structure of CdS by shifting the Fermi level as illustrated in Figure 11c and resulting in metallic films. Consequently, the calculations suggest that S vacancies in the bulk of the CdS film deposited at low temperature may contribute to the observed red-shift of the film band gap down to 2.3 eV and may cause the slowly increasing slope in the Tauc plot before the bandgap absorption energy if the vacancies introduce a spectrum of states within the bandgap. We propose that annealing the 150 °C film in an H_2S atmosphere results in the refilling of the vacancies,

(42) Chen, Z.; Jaramillo, T.; Deutsch, T.; Kleiman-Shwarsctein, A.; Forman, A.; Gaillard, N.; Garland, R.; Takanabe, K.; Heske, C.; Sunkara, M.; McFarland, E.; Domen, K.; Miller, E.; Turner, J.; Dinh, H. *J. Mater. Res.* **2010**, *25*, 3–16.

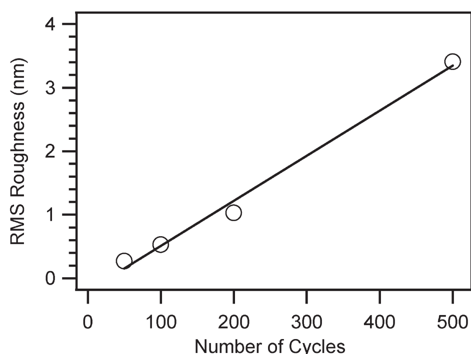

Figure 12. rms roughness versus cycle number of CdS deposited by ALD as determined by AFM. Films were deposited at 150 °C on Si(100).

which increases the bandgap to match the literature value of 2.42 eV and flattens the leading edge of the Tauc plot.

Another possible factor affecting the band gap is the incorporation of hydrogen into the films, which is common for CdS films deposited by CBD; however, in the CBD case the majority of the H atoms were present as interstitials which were removed upon annealing at 150−200 °C. The remaining H atoms were present as CH_x or $Cd(OH)_2$.[34,43] As our films were mostly deposited at or above 150 °C and did not contain O or C impurities, we expect the hydrogen concentration to be negligible at these deposition temperatures, and this is similar to the findings of ZnS deposited with DEZn and H_2S which showed hydrogen impurities of <0.1 at %.[18] Nevertheless, a similar system using trimethylaluminum and water as precursors for Al_2O_3 ALD films did show hydrogen impurity concentrations that decreased with temperature.[28,44] Thus, removal of the light impurities from the 150 °C film upon annealing may contribute to the observed band gap behavior.

AFM and SEM were used to examine the surface morphology of CdS films deposited on Si(100) surfaces as a function of the cycle number at 150 °C. The graph in Figure 12 shows that the rms roughness increases approximately linearly with the number of cycles. This behavior has previously been observed for the DEZn/H_2S ALD system but the roughness is noticeably greater for the CdS system reported herein.[17,18] SEM plan view images of the 100 and 500 cycle samples at 150 °C as shown in Figure 13 delineate two key features of the films due to their thicknesses. First, the 500 cycle film is much rougher, consistent with the AFM results. Second, the surface features appear to be much smaller for the 100 cycle film compared to the 500 cycle film. Further, the 500 cycle film does not appear to be uniformly rough.

The surface morphology was also studied for films deposited at different temperatures. Figure 14 is a plot

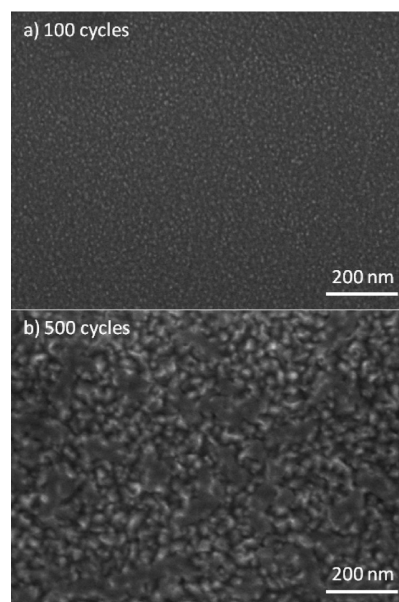

Figure 13. SEM plan view of (a) 100 cycles and (b) 500 cycles CdS deposited at 150 °C on Si(100).

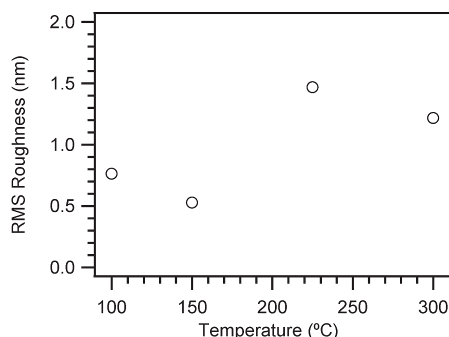

Figure 14. rms roughness versus temperature of CdS deposited by ALD on Si(100) as determined by AFM.

of the rms roughness as a function of temperature. The graph shows that the rms roughness is constant at low temperatures and then rises to a higher value by 225 °C. This trend of an increase around 150 °C is similar to that noted for the wurtzite grain size measured by XRD (Figure 7), leading us to speculate that the increasing presence of wurtzite crystals which are also randomly oriented causes an increase in roughness on the film. On the other hand, DFT simulations provide another possible explanation: if the growth process transitions from a monolayer coverage process to a partial monolayer process at higher temperatures as suggested by the change in dissociation energy of the DMCd precursor (Figure 6), this may also lead to increase in roughness with temperature. A similar growth method has been postulated as the cause of roughness for the related DEZn/H_2S system.[17,18] The SEM plan view images in Figure 15 show 250 cycle films deposited at 100 and 300 °C. Both films show uniform roughness across the surface; however, the 300 °C film is both rougher and contains larger features, consistent with Figure 14.

(43) Krauser, J.; Riedle, T.; Klenk, R.; Klaer, J.; Lux-Steiner, M. C.; Weidinger, A. *Appl. Phys. A: Mater. Sci. Process.* **2000**, *70*, 617–623.
(44) Groner, M. D.; Elam, J. W.; Fabreguette, F. H.; George, S. M. *Thin Solid Films* **2002**, *413*, 186–197.

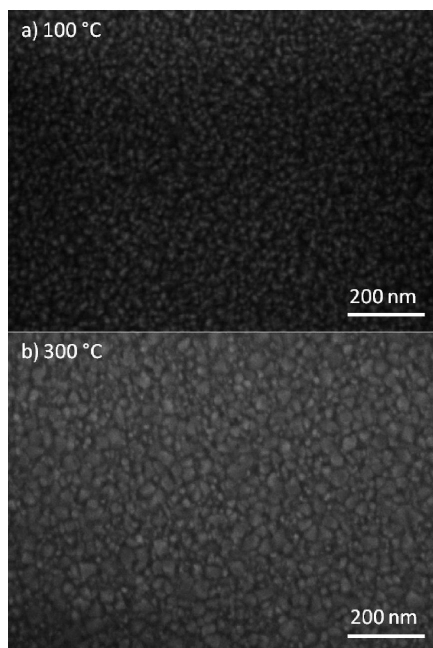

Figure 15. SEM plan view of 250 cycle films deposited at (a) 100 °C and (b) 300 °C on Si(100).

Conclusion

Polycrystalline, near stoichiometric CdS has been deposited by ALD using DMCd and in situ generated H_2S. The film thickness versus cycle number is linear for the temperature range 100−300 °C, and the growth rate is monotonically decreasing with temperature. At 400 °C the deposition is not uniform, and the growth rate varies with the number of cycles and the position on the wafer. Typical saturation behaviors with DMCd pulse time and purge time are observed for this ALD process. DFT calculations suggest that the decreasing growth rate with temperatures occurs because the deposition of material in a submonolayer manner is thermodynamically favored at high temperatures.

XRD and TEM were used to confirm that at temperatures as low as 100 °C, the CdS films were primarily zincblende with wurtzite content; however, the wurtzite character of the films rapidly increased to become the dominant crystal structure by 400 °C. Compared to a similar II−VI metal chalcogenide, the wurtzite nature of the CdS films is much stronger than for ZnS at a given temperature. The TEM images and SAD patterns also establish that crystals are more highly oriented at lower temperatures. Analysis of the fwhm of the XRD patterns using the Scherrer equation shows that the grain size of the zincblende portion of the film increases linearly with temperature while the wurtzite grains are a constant size and then increase more suddenly in size at higher temperatures. This phenomenon may be explained by TEM images showing that smaller wurtzite grains are present because of stacking faults in the cubic phase. Tauc plots obtained from UV−vis measurements were used to confirm that the band gap matches literature values of 2.42 eV. DFT simulations indicate that absorption at lower energies in CdS films may be due to sulfur vacancies, and experiments suggest that sulfur atoms may replace vacancies by annealing in an H_2S atmosphere.

SEM and AFM were used to study the surface morphology as a function of temperature and cycle number. The roughness increases linearly with cycle number (thickness) in a similar fashion to ZnS although CdS is consistently rougher for a given thickness. Surface roughness was confirmed to increase with temperature as well. These surface properties may be due to the growing crystal size, to the increasing mixture of different phases, or to the preference for depositing in a submonolayer manner as suggested by DFT simulations.

We have demonstrated a successful method for ALD of CdS thin films with a good degree of control over crystal phase and morphology with changing growth parameters. Moreover, our results show that CdS deposited by ALD can form the wurtzite phase at temperatures significantly lower than the thermodynamic zincblende-to-wurtzite phase transition temperature. Considering the array of uses for CdS, we believe this study will be applicable to many fields which require deposition of CdS films with tunable material properties.

Acknowledgment. J.R.B. acknowledges funding from the Department of Defense (DoD) through the National Defense Science and Engineering Graduate Fellowship (NDSEG) and from the National Science Foundation (NSF) Graduate Fellowship. J.T.T. acknowledges financial support from the University of Eastern Finland. We also recognize use of the Stanford Nanocharacterization Laboratory (SNL) and of the Center for Polymer Interfaces and Macromolecular Assemblies (CPIMA). The authors gratefully appreciate support from Varian Semiconductor Equipment Associates. The TEM and SAD studies were supported as part of the Center on Nanostructuring for Efficient Energy Conversion, an Energy Frontier Research Center funded by the U.S. Department of Energy, Office of Science, Office of Basic Energy Sciences under Award No. DE-SC0001060.

Supporting Information Available: HRTEM and the corresponding FFT images are available for the 150 and 400 °C films. AFM micrographs for multiple temperatures and thicknesses are also available. This material is available free of charge via the Internet at http://pubs.acs.org.